Received: 31 March 2024 | Revised: 18 November 2024 | Accepted: 1 December 2024

Energy Conversion and Economics

DOI: 10.1049/enc2.70002

国家电网 STATE GRID 国网经济技术研究院有限公司 STATE GRID ECONOMIC AND TECHNOLOGICAL RESEARCH INSTITUTE CO., LTD.

IET The Institution of Engineering and Technology WILEY

ORIGINAL RESEARCH

Characterising the resilience of electro–hydrogen coupled system via convex hull estimation

Siyuan Chang[1] | Gengyin Li[1] | Tiance Zhang[1] | Ming Zhou[1] | Qiteng Hong[2] | Jianxiao Wang[3]

[1]The State Key Laboratory of Alternate Electrical Power System with Renewable Energy Sources, North China Electric Power University, Beijing, China

[2]Department of Electronic and Electrical Engineering (EEE), University of Strathclyde, Glasgow, UK

[3]The National Engineering Laboratory for Big Data Analysis and Applications, Peking University, Beijing, China

Correspondence
Tiance Zhang, The State Key Laboratory of Alternate Electrical Power System with Renewable Energy Sources, North China Electric Power University, Beijing 102206, China.
Email: ncepuztc@ncepu.edu.cn

Qiteng Hong, University of Strathclyde, 204 George Street, Glasgow, G1 1XW, UK.
Email: q.hong@strath.ac.uk

Funding information
Science and Technology Department of Gansu Province, Grant/Award Number: 22ZD6GA032; China Postdoctoral Science Foundation, Grant/Award Number: GZC20230787

Abstract

Frequent outbreaks of severe natural disasters underscore the importance of power system resilience. With high efficiency and rapid response, hydrogen energy can enhance power system resilience during such incidents. Traditional post-event resilience assessment methods, which are event-triggered, focus on a single indicator, leading to an ambiguous portrayal of the power capacity of coupled systems. To address this limitation, based on a two-stage electro–hydrogen coupled model, the concept of electro–hydrogen coupled region (EHCR) is proposed to illustrate the potential relationships between resilience indicators, exploring the accurate power capacity of the coupled system to critical loads during extreme events. The convex hull estimation is employed to determine the EHCR. A max–min diagnostic model is introduced as the convergence criterion for resilience margins. An external cutting-plane algorithm is developed to interactively obtain the EHCR by progressively eliminating non-capacity regions of the current space based on the diagnostic model. The efficacy of the proposed methods is validated through case studies based on an IEEE 30-bus and Belgium 20-node coupled system under ice disaster scenarios.

KEYWORDS
convex hull estimation, electro-hydrogen coupled system, resilience margin, two-stage resilience model

1 | INTRODUCTION

The high incidence of extreme natural disasters resulting from the growing climate crisis presents significant challenges to power systems [1, 2]. In early 2024, a severe ice disaster caused power supply disruptions in Zhejiang, China, with ice thicknesses on transmission lines reaching 25 mm. In 2021, extreme cold temperatures led to a shortage of natural gas supply, triggering a widespread power outage in Texas, USA [3]. These events highlight the vulnerability of power systems during extreme natural disasters, which pose a series of threats to secure and stable operations [4, 5]. Consequently, the concept of resilience has been introduced to characterise the capability of a power system to withstand and recover from low-probability high-risk faults.

Integrated energy systems (IESs) have been widely studied owing to improvements in energy utilisation and adjustable capacity, and they can provide power support and reduce power curtailment during extreme events. In reference [6], load curtailment was reduced by redistributing the loads in a multi-energy distribution system. In reference [7], a two-stage risk-averse restoration method based on a power and water coupled system was proposed. Compared to heat and water energy, hydrogen energy possesses distinctive characteristics such as transportability, ease of production and use, fast refuelling rate, and high energy density [8, 9], making it a valuable resource for

enhancing power system resilience during extreme events. The coupling of hydrogen and electricity can improve operational flexibility and objectives, such as the accommodation of renewable energy sources and reduction of load curtailment, by regulating multiple controllable energy conversion and storage devices [10, 11]. When power system resilience is compromised, hydrogen energy in storage equipment or pipelines can be swiftly converted into power using hydrogen to power (H2P) technology [12, 13].

Extreme events typically exhibit coupled temporal and spatial characteristics. For example, ice disasters and torrential rains exhibit cumulative effects over time, and typhoons move constantly in space. However, it is noteworthy that the current event-triggered resilience assessment methods mainly focus on the power supply level of the resilience curve [14, 15]. Additionally, the resilience level is commonly evaluated using a single indicator at a point in time, neglecting the potential interrelationships between indicators within the power system and coupled systems [16]. Furthermore, the potential of hydrogen energy systems to bolster power system resilience remains underutilised, leading to an insufficient portrayal of the power capacity of electro–hydrogen coupled systems [17, 18].

Furthermore, existing model aggregation and equivalence methods make it difficult to accurately portray the power capacity under extreme events. Reference [19] proposed a robust active dynamic aggregation model for distributed integrated multi-energy systems to describe the maximum feasible region, which is more efficient than KKT-based algorithms. In reference [20], the external properties of the coupled system were equal to the maximum internally connected right-angled hypercube in the flexibly feasible region, which sacrifices the accuracy for the stability of the results. Reference [21] approximated the external properties using a simple generalised Chino polytope. In [22], the external properties of coupled systems were represented by a generalised Chino polyhedral based on the Minkowski method, which does not apply to scenarios with numerous subconstraints and variables. In conclusion, the methods struggle to adapt to the coupled system resilience in scenarios with high dimensions, multiple periods, and heterogeneous energy resources.

To address the aforementioned gaps and challenges, an external cutting-plane generation algorithm was initially proposed to characterise the resilience margin of an electro–hydrogen coupled system, which adapts to high dimensions and multiple periods. Subsequently, a two-stage electro–hydrogen coupled resilience model was built to observe the electro–hydrogen coupled region (EHCR) before and during the incidents. A method based on a second-order cone (SOC) and Taylor series was applied to solve the non-convex constraints. Finally, using ice disasters as the context, the effectiveness of the proposed methods was validated through an IEEE 30-bus and Belgium 20-node coupled system and a coupled system consisting of an actual 102-bus and Belgium 20-node system. The contributions of this study are as follows:

(i) To address the issues of existing resilience assessment methods, the concept of EHCR is proposed to characterise resilience using multiple indicators and a clear power capacity in two stages under extreme events. Compared with traditional methods based on resilience curves, the coupling relationships between resilience indicators can be portrayed through the EHCR, which reveals the cumulative effects of extreme disasters over time. The EHCR not only clarifies how much power capacity can be provided by the hydrogen energy system at a given time point but also answers the question of whether the hydrogen energy system can supply sufficient power capacity to meet the critical load demand under multiple time cross-sections.

(ii) Convex hull estimation is applied to address the high dimensions, multiple periods, and heterogeneous energy resources in coupled systems. A max–min diagnostic model and an external cutting-plane algorithm are introduced to estimate whether the current optimisation space is an EHCR, which is transformed into mixed integer linear programming (MILP) problems that are easily solved by commercial solvers.

(iii) A two-stage electro–hydrogen-coupled model is built to explore the EHCR variation of critical loads in the power system under extreme events. The support of the hydrogen energy system for critical loads is demonstrated, and its capacity is accurately portrayed, which can help the power system achieve rapid restoration.

2 | FRAMEWORK

Most existing resilience assessment methods are based on the resilience triangle [23] and resilience trapezoid [24], which can further quantify how fast the system performance decreases and recovers. This method simulates scenarios within a contingency set to obtain an event-triggered three-stage resilience curve [25]. By analysing characteristics such as the decline rate, duration, and recovery level of the resilience curve, the resilience level of the system is evaluated. These methods concentrate mainly on the system as a whole and ignore the coupling relationships between the variables within the system. For electro–hydrogen coupled systems, the power capacity of the hydrogen system, which can help with emergency dispatch during events and system recovery after disasters, is not considered.

Characterising the EHCR of critical loads is an effective method for revealing the variations in system resilience during disasters. By estimating the convex hull formed by the constraints, an EHCR characterises the potential relationships between the variables and obtains the power capacity of the critical bus. The overall process is illustrated in Figure 1.

In this study, first, a two-stage electro–hydrogen coupled model is built. The model covers the pre- and in-event stages. Subsequently, an efficient solution algorithm for the EHCR and an analytical representation of the resilience margins are proposed. Finally, the capacity of the power and hydrogen systems to withstand critical loads is accurately portrayed under ice disaster scenarios.

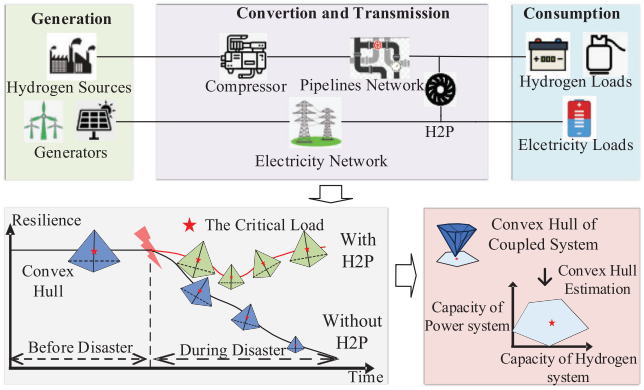

FIGURE 1 Illustration of electro–hydrogen coupled system resilience characterisation based on the EHCR.

3 | ELECTRO–HYDROGEN COUPLED RESILIENT MODEL

3.1 | Objective function of the model

The electro–hydrogen coupled two-stage model is based on a power system and a hydrogen energy system transmission network. The model temporally covers both the pre-event and in-event stages of extreme disasters. In the pre-event stage, the objective is to satisfy the load requirements and minimise operational costs. In the in-event stage, the goal is to minimise load shedding and meet the needs of the critical load. The objective function is formulated using Equation (1).

$$\min \sum_{t\in\Phi^{T1}} C_t^{pre} + \sum_{t\in\Phi^{T2}} C_t^{in} \tag{1}$$

where C_t^{pre} and C_t^{in} represent the costs of the coupled system before and during a disaster, respectively. Φ^{T1} and Φ^{T2} represent the time set of the system before and during a disaster, respectively.

Before the disaster, the coupled system is not affected. The cost mainly includes the operating, start-up, and shutdown costs of the units, and the operating costs of the hydrogen energy system.

$$C_t^{pre} = \sum_{t\in\Phi^{T1}} C_{P,t}^{pre} + \sum_{t\in\Phi^{T1}} C_{H,t} \tag{2}$$

$$C_{P,t}^{pre} = \sum_{g\in\Phi^{G}} \alpha_g P_{g,t}^2 + \beta_g P_{g,t} + c_g s_{g,t} + c^{up} s_{g,t}^{up} + c^{down} s_{g,t}^{down} \tag{3}$$

$$C_{H,t} = \sum_{w\in\Phi^{W}} \alpha_w F_{w,t} + \sum_{h2p\in\Phi^{H2P}} \alpha_{h2p} F_{h2p,t} \tag{4}$$

where $C_{P,t}^{pre}$ represent the cost of the power system before the disaster. α_g, β_g, and c_g are the cost coefficients of the generator g. c^{up} and c^{down} are the start-up and shut-down costs of the generator g. $P_{g,t}$ is the power output of the generator g at time t. $s_{g,t}$, $s_{g,t}^{up}$, and $s_{g,t}^{down}$ are binary variables that represent the state of generator g at time t. If generator g operates at time t, then $s_{g,t} = 1$; otherwise $s_{g,t} = 0$. If generator g starts up or shuts down at time t, then $\frac{s_{g,t}^{up}}{s_{g,t}^{down}} = 1$; otherwise, $\frac{s_{g,t}^{up}}{s_{g,t}^{down}} = 0$. $C_{H,t}$ represents the cost of the hydrogen energy system. Φ^{W} and Φ^{H2P} are the sets of hydrogen source and H2P installations. $F_{w,t}$ and $F_{h2p,t}$ are the output (thousand cubic meters, $10^3 * m^3$) of the gas source and the consumption of $h2p$ at time t. α_w and α_{h2p} are the cost coefficients of hydrogen output and consumption per thousand cubic meters.

During a disaster, lines within the affected area may experience an outage and the units may be triggered because of frequency protection. Regulating the output and reducing load shedding are the primary targets at this stage. The objective is as follows:

$$C_t^{in} = \sum_{t\in\Phi^{T2}} C_P^{in} + \sum_{t\in\Phi^{T2}} C_H \tag{5}$$

$$C_P^{in} = \sum_{g\in\Phi^{G}} \alpha_g P_{g,t}^2 + \beta_g P_{g,t} + c_g s_{g,t} + c^{up} s_{g,t}^{up} + c^{down} s_{g,t}^{down} + \sum_{l\in\Phi^{L}} c^{lost} P_{l,t}^{lost} \tag{6}$$

where C_P^{in} represents the power system cost during a disaster. Φ^{L} is the set of the load l in the power system. c^{lost} is the curtailment of the load l. $P_{l,t}^{lost}$ is the curtailment of load l at time t.

3.2 | Constraints of the power system

3.2.1 | Generator units' operation constraints

Generator units' operation constraints include active and reactive output and ramping constraints. The former is expressed by Equations (7) and (8). The latter is shown in Equation (9).

$$s_{g,t} P_g^{min} \le P_{g,t} \le s_{g,t} P_g^{max} \tag{7}$$

$$s_{g,t} Q_g^{min} \le Q_{g,t} \le s_{g,t} Q_g^{max} \tag{8}$$

$$-R_g \le P_{g,t} - P_{g,t-1} \le R_g \tag{9}$$

where P_g^{min}/P_g^{max} and Q_g^{min}/Q_g^{max} are the minimum and maximum outputs of the active and reactive powers of generator g, respectively. R_g is the ramping limit of generator g. Note that if $s_{g,t} = 0$, the active and reactive outputs of generator g at time t are zero.

3.2.2 | Binary variable constraints related to generators

If load shedding occurs in the power system, the generators are triggered to change their operating status, as shown in Equation (10). Equations (11) and (12) describe the relationships

between the operating status and start-up/shut-down status of the generators.

$$s_{g,t} + o_{g,t} \leq 1 \tag{10}$$

$$s_{g,t} - s_{g,t-1} = s^{\text{up}}_{g,t} - s^{\text{down}}_{g,t} \tag{11}$$

$$s^{\text{up}}_{g,t} + s^{\text{down}}_{g,t} \leq 1 \tag{12}$$

where $o_{g,t}$ is a binary variable that represents the triggering status of unit g at time t. If unit g is triggered at time t, then $o_{g,t} = 1$ and $s_{g,t} = 0$, otherwise $o_{g,t} = 0$ and $s_{g,t} = 0$ or 1. Equation (11) shows that if $s_{g,t} = s_{g,t-1}$, then $s^{\text{up}}_{g,t} = s^{\text{down}}_{g,t} = 0$. If $s_{g,t} - s_{g,t-1} = 1$, then $s^{\text{up}}_{g,t} = 1$ and $s^{\text{down}}_{g,t} = 0$. If $s_{g,t} - s_{g,t-1} = -1$, then $s^{\text{up}}_{g,t} = 0$ and $s^{\text{down}}_{g,t} = 1$.

3.2.3 | Power flow and power balance constraints

The linearised power flow constraints are as follows: If a line experiences an outage during a disaster, its power flow will be zero.

$$P_{ij,t} = g_{ij}\left(U_{i,t} - U_{j,t}\right)/2 - b_{ij}\left(\theta_{i,t} - \theta_{j,t}\right) \tag{13}$$

$$Q_{ij,t} = -g_{ij}\left(U_{i,t} - U_{j,t}\right) - b_{ij}\left(\theta_{i,t} - \theta_{j,t}\right)/2 \tag{14}$$

where $P_{ij,t}$ and $Q_{ij,t}$ are the active and reactive powers of line ij at time t, respectively. g_{ij} and b_{ij} represent the conductance and susceptance values of line ij, respectively. $U_{i,t}$ and $\theta_{i,t}$ represent the voltage and phase angle of node i at time t. Equations (15)–(18) illustrate the constraints.

$$U_i^{\min} \leq U_{i,t} \leq U_i^{\max} \tag{15}$$

$$\theta_i^{\min} \leq \theta_{i,t} \leq \theta_i^{\max} \tag{16}$$

$$-k_{ij,t}P_{ij}^{\max} \leq P_{ij,t} \leq k_{ij,t}P_{ij}^{\max} \tag{17}$$

$$-k_{ij,t}Q_{ij}^{\max} \leq Q_{ij,t} \leq k_{ij,t}Q_{ij}^{\max} \tag{18}$$

where $U_i^{\min}$ and $U_i^{\max}$ are the lower and upper limits of voltage at node i., respectively. $\theta_i^{\min}$ and $\theta_i^{\max}$ are the lower and upper limits of phase angle at node i, respectively. $P_{ij}^{\max}$ and $Q_{ij}^{\max}$ are the maximum allowable values of the active and reactive power of line ij, respectively. $k_{ij,t}$ is a binary variable describing the operating status of line ij at time t. If line ij experiences an outage at time t, then $k_{ij,t} = 0$. Otherwise $k_{ij,t} = 1$. When $k_{ij,t} = 0$, the active and reactive powers in line ij are zero.

$$-\sum_{i,j\in\Phi^{\text{B}}} P_{ij,t} + \sum_{g\in\Phi^{\text{G}}} P_{g,t} + \sum_{h2p\in\Phi^{\text{H2P}}} P_{h2p,t} = \sum_{l\in\Phi^{\text{L}}}\left(P_{l,t} - P^{\text{lost}}_{l,t}\right) \tag{19}$$

$$-\sum_{i,j\in\Phi^{\text{B}}} Q_{ij,t} + \sum_{g\in\Phi^{\text{G}}} Q_{g,t} + \sum_{h2p\in\Phi^{\text{H2P}}} Q_{h2p,t} = \sum_{l\in\Phi^{\text{L}}}\left(Q_{l,t} - Q^{\text{lost}}_{l,t}\right) \tag{20}$$

where Φ^{B} is the set of buses in the power system. $P_{h2p,t}$ and $Q_{h2p,t}$ are the active and reactive outputs of the H2P installations at time t, respectively. $P_{l,t}$ and $Q_{l,t}$ represent the load demands of load l at time t.

3.2.4 | Load curtailment constraints

During a disaster, the power capacity of the coupled system is significantly reduced owing to damage to the transmission lines and load shedding of the generators. We define the reduction in capacity as load curtailment. The load-curtailment constraints are given by Equations (21) and (22), respectively.

$$0 \leq P^{\text{lost}}_{l,t} \leq P_{l,t}, \forall t \in \Phi^{\text{T2}} \tag{21}$$

$$0 \leq Q^{\text{lost}}_{l,t} \leq Q_{l,t}, \forall t \in \Phi^{\text{T2}} \tag{22}$$

3.3 | Constraints of hydrogen energy system

Similar to a power system, a hydrogen energy system has source output, pipeline flow, and nodal flow balance constraints. The hydrogen-energy model used in this study was built on a transmission network. Unlike a power system, the transmission network of a hydrogen system is often radial, whereas the distribution network is usually circular [26]. Owing to the high pressure, long transmission distance, and equipment, such as compressors, in the transmission network, the direction of hydrogen flow in the pipelines is usually fixed and seldom changes. Therefore, the direction of the hydrogen flow was not considered, and the flow was approximated using the well-known Weymouth equation, as shown in Equation (23). The source hydrogen output, node pressure, and transmission capacity of the pipelines were constrained by their upper and lower limits, as expressed in Equations (24)–(26).

$$F_{mn,t} = K_{mn}\sqrt{\pi_m^2 - \pi_n^2} \tag{23}$$

$$F_w^{\min} \leq F_{w,t} \leq F_w^{\max} \tag{24}$$

$$\pi_m^{\min} \leq \pi_{m,t} \leq \pi_m^{\max} \tag{25}$$

$$F_{mn}^{\min} \leq F_{mn,t} \leq F_{mn}^{\max} \tag{26}$$

where $F_{mn,t}$ is the average hydrogen flow in pipe mn at time t. K_{mn} is the Weymouth constant of pipe mn. $\pi_{m,t}$ represents the pressure of node m at time t. $F_w^{\min}$ and $F_w^{\max}$ are the lower and upper limit of hydrogen output values of source w, respectively. $\pi_m^{\min}$ and $\pi_m^{\max}$ are the lower and upper limit of the pressure of

node m, respectively. $F_{mn}^{\min}$ and $F_{mn}^{\max}$ are the lower and upper flow allowances of pipe mn, respectively.

Unlike power systems, hydrogen energy can be stored in pipelines in hydrogen energy systems. This effect is described by Equations (27) and (28).

$$F_{mn,t} = \left(F_{mn,t}^{\text{in}} + F_{mn,t}^{\text{out}}\right)/2 \tag{27}$$

$$F_{mn,t}^{\text{in}} - F_{mn,t}^{\text{out}} = \begin{cases} \mathcal{D}_{mn}\left(\frac{\pi_{m,t}+\pi_{n,t}}{2} - \frac{\pi_{m,t-1}+\pi_{n,t-1}}{2}\right), t = 1 \\ \mathcal{D}_{mn}\left(\frac{\pi_{m,t}+\pi_{n,t}}{2} - \frac{\pi_{m,t-1}+\pi_{n,t-1}}{2}\right) + F_{mn,t-1}^{\text{in}} - F_{mn,t-1}^{\text{out}}, t \geq 2 \end{cases} \tag{28}$$

where $F_{mn,t}^{\text{in}}$ and $F_{mn,t}^{\text{out}}$ are the hydrogen inflow and outflow of pipeline mn at time t, respectively. $\mathcal{D}_{mn}$ is the storage constant of pipeline mn. Equation (28) indicates the time-coupled relationships among storage capacity, hydrogen flow, and node pressure.

The nodal balance of a hydrogen energy system indicates that the amount of hydrogen flowing to a node is equal to the amount flowing out, as shown in Equation (29).

$$-\sum_{m,n\in\Phi^{\text{N}}} F_{mn,t}^{\text{in}} + \sum_{m,n\in\Phi^{\text{N}}} F_{mn,t}^{\text{out}} + \sum_{w\in\Phi^{\text{W}}} F_{w,t} - \sum_{h2p\in\Phi^{\text{H2P}}} F_{h2p,t} = \sum_{h\in\Phi^{\text{H}}} F_{h,t} \tag{29}$$

where Φ^{N} is the set of nodes in the hydrogen system. Φ^{H} is the load set for the hydrogen system. Φ^{H2P} represents the H2P installation set of the hydrogen system. $F_{h,t}$ is the hydrogen consumption of the load demand.

In addition, compressor constraints must be considered because of the long-distance transmission and high node pressure.

$$\pi_{q,t} = K_{pq}\,\pi_{p,t} \tag{30}$$

$$\pi_{q,t} \geq \pi_{p,t} \tag{31}$$

where K_{pq} is the compression factor of the compressor pq. $\pi_{p,t}$ and $\pi_{q,t}$ are the node pressure at the beginning and the end of compressor pq.

Equation (23) is non-linear, which makes it difficult to solve and portray the resilience margins of the coupled system during a disaster. A method based on SOC relaxation and the Taylor series was applied to Equation (23). The detailed procedure is presented in Appendix A1.

3.4 | System coupling constraints

The load of the coupled system consists of hydrogen, energy, and electricity. Under the premise of meeting the load demand, users can choose the energy type based on supply capacity, price, and other factors. In this study, electricity (MW) was used as the energy equivalent to uniformly represent the load demand.

$$\sum_{l\in\Phi^{\text{L}}} P_{l,t} = \lambda S_t \tag{32}$$

$$\sum_{h\in\Phi^{\text{H}}} P_{h,t} = (1-\lambda)\,S_t \tag{33}$$

where S_t is the total active load required for the coupled system. λ is the proportion of active load in the power system. $P_{h,t}$ stands for the active load demand of the hydrogen load h at time t, which is transformed into hydrogen energy, as shown in Equation (34).

$$F_{h,t} = \zeta^{\text{P2G}}\,\frac{P_{h,t}}{\text{LHV}^{\text{H}_2}} \tag{34}$$

where ζ^{P2G} represents the efficiency of converting electricity into hydrogen. LHV^{H_2} is the low-heat value of hydrogen under standard conditions.

At the coupling points, hydrogen energy can be converted into electricity for the demand of loads through H2P. The constraints of the conversion process are as follows.

$$P_{h2p,t} = \xi^{\text{H2P}}\,F_{h2p,t}\cos\varphi \tag{35}$$

$$Q_{h2p,t} = \xi^{\text{H2P}}\,F_{h2p,t}\sin\varphi \tag{36}$$

where $P_{h2p,t}$ and $Q_{h2p,t}$ are the active and reactive power output of $h2p$ at time t, respectively. ξ^{H2P} represents the efficiency of converting hydrogen into electricity. $F_{h2p,t}$ is the hydrogen consumption of $h2p$ at time t. $\cos\varphi$ represents the power factor of $h2p$.

To meet the normal supply of hydrogen load and prevent H2P from converting too much hydrogen into electricity, further constraints were introduced based on the H2P output constraints.

$$P_{\text{H2P,min}} \leq P_{h2p,t} \leq P_{\text{H2P,max}} \tag{37}$$

$$Q_{\text{H2P,min}} \leq Q_{h2p,t} \leq Q_{\text{H2P,max}} \tag{38}$$

$$\sum_{h2p\in\Phi^{\text{H2P}}} P_{h2p,t} \leq \sum_{l\in\Phi^{\text{L}}} \varsigma_l^{h2p} P_{l,t} \tag{39}$$

where $P_{\text{H2P,min}}/P_{\text{H2P,max}}$ and $Q_{\text{H2P,min}}/Q_{\text{H2P,max}}$ represent the lower and upper active and reactive power outputs of H2P, respectively. ς_l^{h2p} is the restriction factor of $P_{h2p,t}$.

4 | EHCR THROUGH HULL ESTIMATION

4.1 | Definition of EHCR

Provided that the dispatch problem of the electro–hydrogen coupled system has solutions, the feasible region of the problem should be a high-dimensional hull consisting of all the feasible solutions [27]. The operations of coupled systems are affected by the emergence and development of extreme events. The scheduling means available to the coupled system, that is, the feasible solutions to the dispatch problems, are reduced, and the volume of the dimensional hull is deduced. Thus, changes in the hull can respond to changes in the operating state of the system, and subsequently, to the resilience of the system. In this study, the EHCR is the projection of a high-dimensional convex hull onto a bus or node within a system [28]. The internal constraints of the coupled system can be simplified as Equation (40).

$$\phi = \left\{ x, y \middle| \boldsymbol{A}x + \boldsymbol{B}y \le \boldsymbol{C} \right\} \tag{40}$$

where ϕ represents the high-dimensional convex hull formed by constraints. x represents the projection parameter. y refers to other variables in the coupled system. For example, if the focus is on the power capacity of the critical bus, then the injected power can be regarded as the projection parameter. The other variables, such as the voltage and phase angle, are y parameters. $\boldsymbol{A}$ and $\boldsymbol{B}$ are the coefficient matrices corresponding to x and y. $\boldsymbol{C}$ represents the constant terms in the system.

It is noteworthy that the operational status of a coupled system changes over time during a disaster. The security of a bus or node at a given time can only reflect the operational state of an internal variable, ignoring dynamic changes between indicators. The EHCR is then introduced to observe the potential connections between different indicators of system resilience. According to the convex hull projection theory, the essence of an EHCR is the projection from a high-dimensional hull into a low-dimensional space that is independent of y but related to x. The set of regions can be expressed using Equation (41).

$$\Omega(x) = P_x(\phi) = \{x | \boldsymbol{A}x \le \boldsymbol{C} - \boldsymbol{B}y\} \tag{41}$$

Because projection is a linear process, the projection result of a high-dimensional convex hull remains convex, and the EHCR after projection can be described by a set of linear inequalities, as expressed in Equation (42).

$$\Omega(x) = \{x | \boldsymbol{D}x \le d\} \tag{42}$$

where $\boldsymbol{D}$ and d are boundary variables related to the EHCR. The essence of portraying the EHCR is to solve the $\boldsymbol{D}$ and d variables.

4.2 | Estimation of resilience margins

To determine the margins of the EHCR, all points on the projection plane must be evaluated to judge whether they are inside the EHCR. Thus, any point x_0 is chosen and an optimisation problem is introduced to determine whether $\boldsymbol{\Omega}(x)$ is an empty set, as Equation (43) shows.

$$\begin{aligned} & f(x) = \min I_{\mathrm{I}}^{\mathrm{T}} s^{\mathrm{I}} + I_{\mathrm{O}}^{\mathrm{T}} s^{\mathrm{O}} \\ s.t. & \begin{cases} \boldsymbol{B}y + I_I^{\mathrm{T}} s^{\mathrm{I}} - I_O^{\mathrm{T}} s^{\mathrm{O}} \le \boldsymbol{C} - \boldsymbol{A}x_0 \\ s^{\mathrm{I}}, s^{\mathrm{O}} \ge 0 \end{cases} \end{aligned} \tag{43}$$

where s^{I} and s^{O} are the inside and outside positive relaxation variables, respectively, which can be considered operational adjustments to the system. $I_{\mathrm{I}}^{\mathrm{T}}$ and $I_{\mathrm{O}}^{\mathrm{T}}$ are unit vectors corresponding to s^{I} and s^{O}, respectively. The optimisation aims to minimise the sum of $I_{\mathrm{I}}^{\mathrm{T}} s^{\mathrm{I}} + I_{\mathrm{O}}^{\mathrm{T}} s^{\mathrm{O}}$, that is, to minimise the influence on the system operational status. If the operating point satisfies the constraints and is within the EHCR, the operational status needs not to be changed, and $f(x) = 0$. If $f(x) > 0$, then either s^{I} or s^{O} must be positive, which indicates that x_0 does not satisfy the operation constraints and the system needs to be adjusted. The conclusion is that the set $\boldsymbol{\Omega}$ of x being non-empty is equivalent to $f(x) = 0$.

Proceeding from the point to the surface, to further characterise the maximum EHCR of buses and the maximum output of the hydrogen energy system, Equation (43) can be written in the form of a max–min bilayer optimisation problem, as shown in Equation (44).

$$\begin{aligned} & f(x) = \max_{x} \min_{s^{\mathrm{I}}, s^{\mathrm{O}}, y} s^{\mathrm{I}} + s^{\mathrm{O}} \\ s.t. & \begin{cases} \boldsymbol{B}y + s^{\mathrm{I}} - s^{\mathrm{O}} \le \boldsymbol{C} - \boldsymbol{A}x \\ \forall x \in \Psi, \exists y \\ s^{\mathrm{I}}, s^{\mathrm{O}} \ge 0 \end{cases} \end{aligned} \tag{44}$$

The current operation space Ψ is assumed, and whether the outermost point in Ψ is inside the set $\boldsymbol{\Omega}$ can be judged. If the outermost point is inside $\boldsymbol{\Omega}$, then $\Psi \subseteq \boldsymbol{\Omega}$ and the current operation space is a part of the resilience region. However, it is difficult for the existing solvers to solve these problems, as shown in Equation (42). A dual transformation is introduced to substitute the *min* problem in Equation (44), as Equation (45) shows.

$$\begin{aligned} & f(x) = \max_{x, z} \mathrm{z}^{\mathrm{T}} (\boldsymbol{C} - \boldsymbol{A}x) \\ s.t. & \begin{cases} \boldsymbol{B}^{\mathrm{T}} z = 0 \\ -1 \le z \le 0 \\ \boldsymbol{D}x \le d \end{cases} \end{aligned} \tag{45}$$

where z is the dual variable of y. According to the relationship between the dual problem and original problem, the optimal solution of Equation (45) is no greater than the minimum solution of Equation (44). When $f(x) = 0$, Equation (45) can be expressed as follows.

$$z^{\mathrm{T}} (\boldsymbol{C} - \boldsymbol{A}x) \le 0 \tag{46}$$

When x varies in the EHCR, the optimal solution z reaches extreme values in the dual space, that is, the vertex of space

$\boldsymbol{Z} = \{z|\boldsymbol{B}^{\mathrm{T}}z = 0, -1 \le z \le 0\}$. The convex-hull expression of the EHCR in the space can be deduced from Equation (46) as Equation (47).

$$\Omega = \left\{x|z_v^{\mathrm{T}}\boldsymbol{A}x \ge z_v^{\mathrm{T}}\boldsymbol{C}\right\} \tag{47}$$

where z_v^{T} is the vertex of z in the dual space. The key to portraying the EHCR is solving z_v^{T}.

4.3 | External cutting-plane algorithm

To find the largest EHCR, all the resilience margins of the convex hull must be determined. However, electro–hydrogen coupled systems are highly dimensional and contain a large number of redundant constraints. Traditional methods based on enumeration or internal traversal have difficulty searching all the margins and may result in a dimensional explosion. To address this issue, an external cutting-plane algorithm is proposed to represent the EHCR. The main idea of the algorithm is to obtain the resilience margin in a large space that contains the EHCR and progressively excise the non-EHCR part from the outside. Based on incremental cutting and approximation from the outside, the EHCR can be portrayed quickly. Thus, issues such as the repeated generation of margins and missing boundaries are avoided, and the problem of large-scale high-dimensional feasible region dimensionality disaster is solved to an extent. The detailed solution algorithm is presented in Appendix A2.

4.4 | Process of solving the EHCR

The overall flow for solving the EHCR is proposed based on the algorithm described in Section 4.3. The flowchart is as follows. (Figure 2)

To solve the margin of the EHCR, an initial space Ψ is set first, which is large enough to contain the precise security region. Then, Equation (A5) is solved according to the current space Ψ. If the value f of the objective is larger than the allowed error σ, a cutting plane is achieved to update Ψ. The loop will not stop until $f \le \sigma$. The output space Ψ is the accurate EHCR of the coupled system.

5 | CASE STUDIES

Modified models based on the IEEE 30-bus and Belgium 20-node coupled system were used to assess the effectiveness of the proposed algorithm in representing the EHCR of critical loads in power systems during ice disasters. The calculations were written and tested on a laptop computer with a 2.4 GHz CPU and 16 GB RAM. The optimisation calculation tool was IBG ILOG CPLEX 12.9, and the programming platform was MATLAB R2021a.

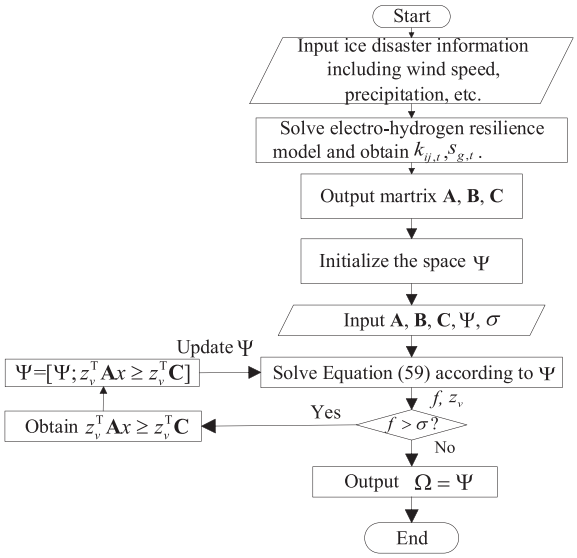

FIGURE 2 Flowchart of the solving model and external cutting-plane algorithm.

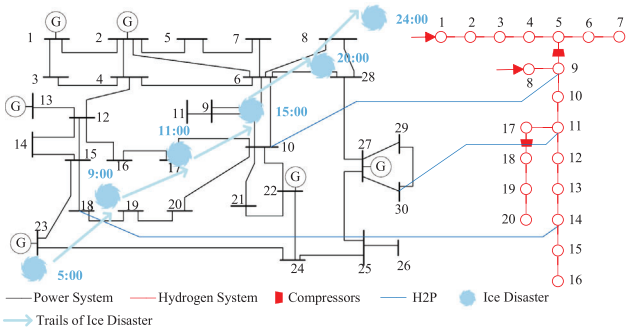

FIGURE 3 Topology chart of the electro–hydrogen coupled system.

TABLE 1 Coupling relationships between two systems.

Serial number	Bus	Node
1	10	9
2	18	14
3	30	11

5.1 | Modified electro–hydrogen coupling system

The topology of the modified electro–hydrogen coupled system is shown in Figure 3. The power system comprises 30 buses, 42 branches, and 6 generator units, with parameters set according to the MATPOWER 6.0 standard case. The hydrogen energy system includes 2 hydrogen sources, 20 nodes, 17 pipelines, and 2 compressors [29]. The improved coupling relationship based on [30] is listed in Table 1. The blue arrow indicates the movement path of the ice disaster, and the critical loads are located at bus 10, where the active and reactive powers are 138 MW and 68.8 MVar, respectively.

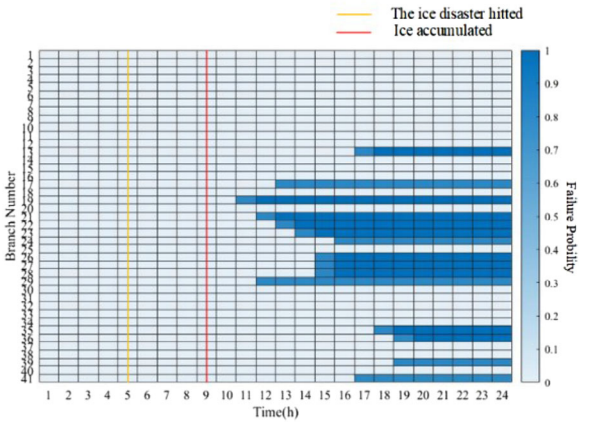

FIGURE 4 Heatmap of outage lines' probability.

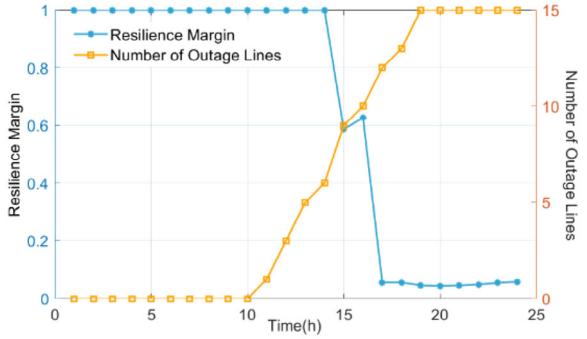

FIGURE 5 Line graph of outage lines' number and critical bus resilience margins.

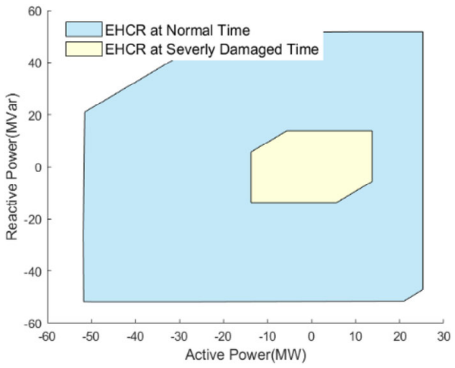

FIGURE 6 EHCR of the critical bus at normal time and severely damaged time.

The impact of the ice disaster on transmission lines can be described using a vulnerability model [31]. The size of the power system was assumed to be 300 ∗ 300 km^2. The ice disaster occurred at a speed of 60 km/h. The impact area of the ice disaster was a circle with a radius of 100 km and a severe impact with a radius of 50 km. The wind speed was 10 m/s, and the precipitation was 80 mm/h in the severely affected areas. Finally, the probability of outage lines at each moment was determined. A heat map of the outage lines is shown below. (Figure 4)

In this study, to simplify the consideration of operational uncertainty, it is assumed that if the probability is greater than 0.8, the transmission line is in an outage. Then, information about outage lines during an ice disaster can be obtained, which is necessary to portray the resilience margin and EHCR of critical loads.

5.2 | EHCR under ice disasters

To visualise the dynamics of the EHCR during the ice disaster, this section only portrays the EHCR of the power system without considering the capacity of the hydrogen energy system. During the disaster, the resilience margin of the critical loads changed as indicated below.

As can be observed, in the early stages of the disaster, few lines experience outage, and the ability to meet the power supply and critical loads is unaffected. As the ice disaster develops and continues, lines within affected areas begin to be in outage, and the resilience margin of the critical bus narrows and reaches its lowest point of less than 5% at 20:00. Thus, the resilience of the power system is significantly affected. The EHCR at 10:00 and 20:00 are shown below. (Figure 5)

Figure 6 shows that the resilience region reflects the impact on the resilience of the power system during an ice disaster. The EHCR is not a regular rectangle, but an irregularly shaped convex polygon, indicating that there are coupling relationships between the injected active and reactive powers of the critical load. It can be observed that in the worst case at 20:00, there is a significant loss in the supply capacity at the critical bus because after 17:00, only two of the six transmission lines directly connected to critical bus 10 remain: line 9–10 and line 10–20. Some generator buses, such as bus 22, are islanded and are unable to provide power. In this transmission-resource-limited situation, it is difficult for the generator buses to supply power to bus 10 directly, resulting in a severe shortage.

5.3 | EHCR Considering H2P

Hydrogen energy is characterised by high energy density, high conversion efficiency, and fast responsiveness. In a scenario of low resilience and excessive load shedding at the critical bus, the H2P of the hydrogen energy system can respond quickly to support critical loads. With H2P support, the resilience margin of the critical loads changes, as shown in Figure 7.

Compared with the resilience margin without H2P, the resilience margin with H2P support improves significantly. In the worst-case scenario at 20:00, the resilience margin of the critical loads is higher than 40%, which is much greater than that in the scenario without H2P support. The EHCR at 20:00 in the two scenarios is shown in Figure 8.

Compared to the EHCR without H2P, the EHCR with H2P is more irregular in shape, indicating that more coupling constraints were projected as a result of the electro–hydrogen coupled system. It can be clearly observed that the capacity of the coupled system to supply critical loads is significantly

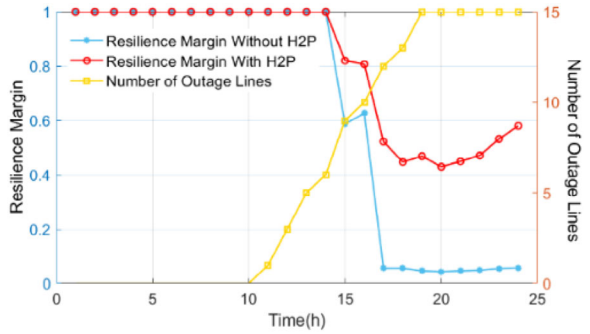

FIGURE 7 Comparison of resilience margins with and without H2P.

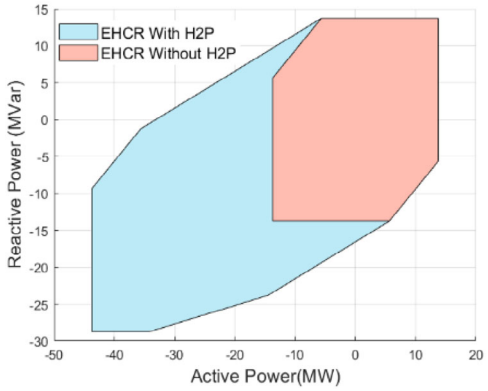

FIGURE 8 Resilience region of critical loads in two scenarios.

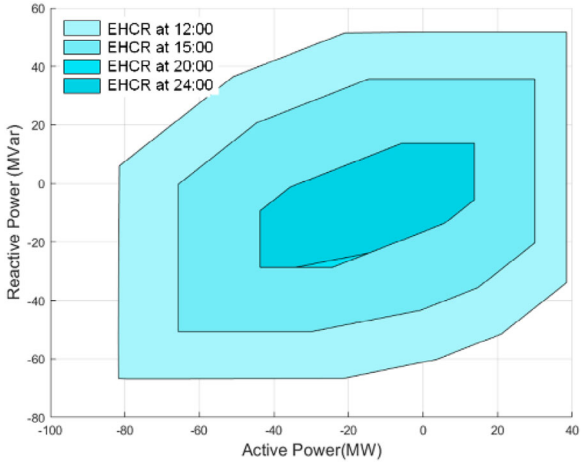

FIGURE 9 Variation of EHCR at four times.

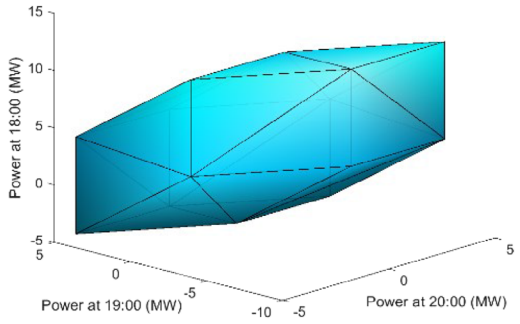

FIGURE 10 Time-coupled EHCR of the power from stored hydrogen.

improved by the H2P support. The EHCR represents the power capacity that can be converted from hydrogen energy through H2P. Meanwhile, the resilience margins of the injected power EHCR to the critical loads are clarified. If the variables of the constraints corresponding to the margins of the EHCR can be determined, then timely adjustments can be made to the system resilience.

Four scenarios were selected to demonstrate the EHCR variation in the load capacity of the critical bus with H2P. These variations are illustrated in Figure 9.

Figure 10 illustrates the time-coupling characteristics of the critical-load injected power in the power system, considering the hydrogen storage effect. The time-coupling constraints at 18:00, 19:00, and 20:00 of the power converted from hydrogen stored in the pipelines are portrayed. It can be observed that the EHCR appears as an irregular convex hull. If the current operation point of the coupled system is outside the EHCR, the stored hydrogen cannot meet the demand of the system, and hydrogen energy must be dispatched from the hydrogen sources.

5.4 | EHCR Considering load constraints

Compared to the EHCR without H2P, the EHCR with H2P at noon is similar to that at 10:00, indicating that the capacity of H2P is almost negligible when no faults or disturbances occur in the power system. In this case, the main purpose of operation is to satisfy the load demand of the subsystems. As the disaster develops and continues, the capacity to support critical loads is weakened but remains at a certain level with H2P. In scenarios of severe faults on lines related to the critical bus, or even if the critical bus becomes islanded, H2P can respond to and meet the partial need for critical loads.

Furthermore, to accurately portray the active power capacity of H2P and the power system, the resilience regions of the active power support of H2P and the power system at 20:00 is portrayed in Figure 11.

The potential relationships between the active power capacity of the power system and the capacity of H2P are shown in Figure 11. It can be observed that the active power capacity of the electro–hydrogen coupled system exhibits an irregularly shaped polygon owing to the load constraints. In conclusion, the EHCR can be used to reflect the influence of scenario evolution on the resilience margin of the power system and the coupling relationship between different variables, in addition to characterising the coupling influence of multiple types of security indicators on critical loads, which fits the power system resilience problem very well.

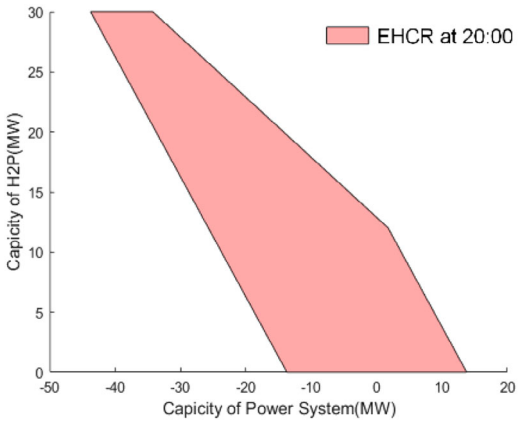

FIGURE 11 Active power EHCR of the coupled system.

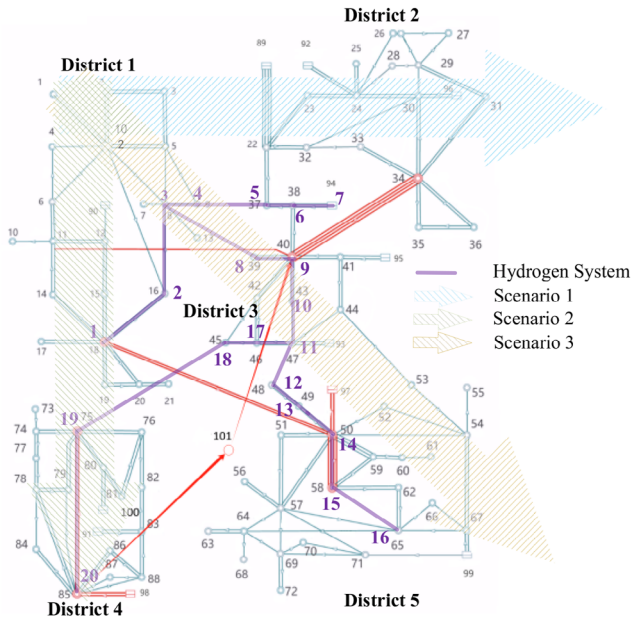

FIGURE 12 Different scenarios based on actual 102-bus and Belgium 20-node coupled system.

5.5 | Actual 102-Bus power system

The electro–hydrogen coupled system based on an actual 102-bus transmission network in China and a Belgium 20-node network is shown in Figure 12. Three ice disaster paths were set to calculate the load curtailment in different scenarios.

The ice disaster arrives at 1 AM and the parameters are equal to those presented in Section 5.1. Generator trips and line outages occur sequentially during the ice disaster. Critical loads are located at buses 40, 43, and 47 in district 3. The coupled relationships are listed in Table 2.

As be observed in Figure 13, the resilience margin remains at a high level in Scenarios 1 and 2, in which the critical load is not affected. In Scenario 3, the resilience margin drops sharply. However, it ultimately remains above 60%, indicating that the hydrogen energy system plays a role in the power supply capacity.

TABLE 2 Coupling relationships between two systems.

Serial number	Bus	Node
1	40	9
2	75	19
3	47	11

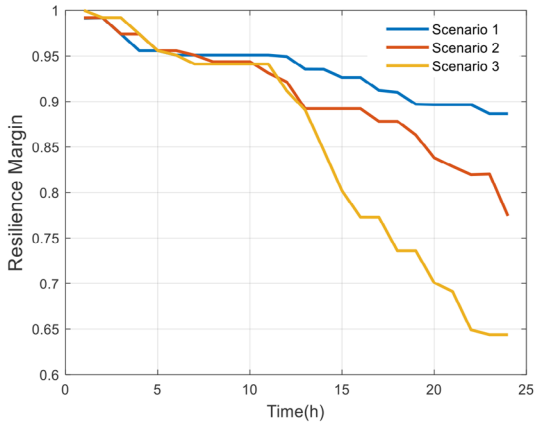

FIGURE 13 Resilience margin under three scenarios.

TABLE 3 Solving time of the cases.

Number	Case title	Solution time(s)
1	IEEE 30-Belgium 20	19.062
2	Actual 102-Belgium 20–1	28.687
3	Actual 102-Belgium 20–2	27.158
4	Actual 102-Belgium 20–3	32.942

The solving times for the different cases are listed in Table 3. As the size of the coupled system increases, the solution time of the model remains within an acceptable limit, indicating that the model is suitable for the computational requirements of a large-scale system.

The performance of the enumeration, multiparameter programming (MP), and proposed methods are listed in Table 4. The enumeration requires less time when searching for directions, but the error makes it difficult to meet the dispatch requirements. As the search directions increase, the computational time increases significantly. The time required by the MP method is much longer than that of the other two algorithms

TABLE 4 Performance of the three algorithms in Scenario 3.

Methods	Direction	Error(%)	Time(s)
Enumeration	16	9.05	140.462
	64	3.24	3548.315
MP	/	/	2039.572
Proposed algorithm	/	/	32.942

and is affected by several constraints, which makes it difficult for this method to adapt to large-scale problems. The algorithm proposed in this study has a distinct advantage in terms of computational efficiency for large-scale coupled problems.

6 | CONCLUSION

In this study, the concept of EHCR is proposed to address the issue of insufficient consideration of the coupled effects between multiple resilience indicators and the ambiguity of the coupled system capacity in existing resilience studies. A two-stage electro–hydrogen coupled system was built, and several load constraints were set to investigate the potential influence of the load constraints on the H2P capacity.

Based on case studies using electro–hydrogen coupled systems under ice disaster scenarios, the following points are demonstrated. (i) The EHCR can reflect the capacity of the power system and hydrogen energy system for critical loads during disasters, which can provide effective information for emergency dispatch. (ii) The coupling relationships between the power system and hydrogen energy system can enhance the resilience of the power system, and the EHCR can not only portray the power capacity of the coupled system, but also show the variation of H2P to critical loads over multiple periods. (iii) The potential relationships among multiple resilience indicators are reflected through the EHCR, which can express the variation trends of resilience during extreme disasters.

In our future work, two directions are worth further exploration: (i) consideration of the inertia support to power systems through H2P and power system frequency response constraints. (ii) Recovery strategies for the coupled system after a disaster, accelerating resilience recovery and ensuring the survival of critical loads.

CONFLICT OF INTEREST STATEMENT

The authors declare no conflicts of interest.

DATA AVAILABILITY STATEMENT

Data sharing is not applicable to this article as no new data were created or analyzed in this study.

ORCID

Siyuan Chang https://orcid.org/0009-0009-6095-3974

REFERENCES

1. Pearson, J., Wagner, T., Delorit, J., et al.: Meeting temporary facility energy demand with climate-optimized off-grid energy systems. IEEE Open Access J. Power and Energy 7, 203–211 (2020)
2. Hussain, H.M., Narayanan, A., Nardelli, P.H.J., et al.: What is energy Internet? concepts, technologies, and future directions. IEEE Access 8, 183127–183145 (2020)
3. Zhang, G., Zhong, H., Tan, Z., et al.: Texas electric power crisis of 2021 warns of a new blackout mechanism. CSEE J. Power and Energy Syst. 8(1), 1–9 (2022)
4. Lu, J., Zeng, M., Zeng, X., et al.: Analysis of ice-covering characteristics of china hunan power grid. IEEE Trans. Ind. Appl. 51(3), 1997–2002 (2015)
5. Huang, W.: Preventive scheduling for reducing the impact of glaze icing on transmission lines. IEEE Trans. Power Syst. 37(2), 1297–1310 (2022)
6. Mu, C., et al.: Multi-objective interval optimization dispatch of microgrid via deep reinforcement learning. IEEE Trans. Smart Grid 15(3), 2957–2970 (2024)
7. Yang, Y., Li, Z., Mandapaka, P.V., Lo, E.Y.M.: Risk-averse restoration of coupled power and water systems with small pumped-hydro storage and stochastic rooftop renewables. Appl. Energy 339, 120953 (2023)
8. Abomazid, M., El-Taweel, N.A., Farag, H.E.Z.: Optimal energy management of hydrogen energy facility using integrated battery energy storage and solar photovoltaic systems. IEEE Trans. Sustainable Energy 13(3), 1457–1468 (2022)
9. Li, J., Li, G., Ma, S., et al.: Modeling and simulation of hydrogen energy storage system for power-to-gas and gas-to-power systems. J. Mod. Power Syst. Clean Energy 11(3), 885–895 (2023)
10. Weiming, L., Jiekang, W., Jinjian, C., et al.: Capacity allocation optimization framework for hydrogen integrated energy system considering hydrogen trading and long-term hydrogen storage. IEEE Access 11, 15772–15787 (2023)
11. Han, J., Wang, J., He, Z., et al.: Hydrogen-powered smart grid resilience. Energy Convers. Econ. 4, 89–104 (2023)
12. Ge, P., Hu, Q., Wu, Q., et al.: Increasing operational flexibility of integrated energy systems by introducing power to hydrogen. IET Renewable Power Gener. 14, 372–380 (2020)
13. Chapman, A., Nguyen, et al.: Hydrogen penetration and fuel cell vehicle deployment in the carbon constrained future energy system. IET Electr. Syst. Transp. 10, 409–416 (2020)
14. Dobson.: Models, metrics, and their formulas for typical electric power system resilience events. IEEE Trans. Power Syst. 38(6), 5949–5952 (2023)
15. Mujjuni, F., Betts, T.R., Blanchard, R.E.: Evaluation of power systems resilience to extreme weather events: a review of methods and assumptions. IEEE Access 11, 87279–87296 (2023)
16. Wang, Y.: A resilience assessment framework for distribution systems under typhoon disasters. IEEE Access 9, 155224–155233 (2021)
17. Haggi, H., Sun, W., Fenton, J.M., et al.: Proactive rolling-horizon-based scheduling of hydrogen systems for resilient power grids. IEEE Trans. Ind. Appl. 58(2), 1737–1746 (2022)
18. Hou, H., Liu, P., Xiao, Z., et al.: Capacity configuration optimization of standalone multi-energy hub considering electricity, heat and hydrogen uncertainty. Energy Convers. Econ. 2, 122–132 (2021)
19. Zhao, H.: Active dynamic aggregation model for distributed integrated energy system as virtual power plant. J. Mod. Power Syst. Clean Energy 8(5), 831–840 (2020)
20. Zhao, L., Zhang, W., Hao, H., et al.: A geometric approach to aggregate flexibility modeling of thermostatically controlled loads. IEEE Trans. Power Syst. 32(6), 4721–4731 (2017)
21. Müller, F.L., Szabó, J., Sundström, O., et al.: Aggregation and disaggregation of energetic flexibility from distributed energy resources. IEEE Trans. Smart Grid 10(2), 1205–1214 (2019)
22. Bao, S., Lei, X., Abulizi, J., et al.: Depiction and aggregation for flexible regulation capability of multi-energy system considering nonconvex operation characteristics. Autom. Electr. Power Syst. 47(15), 55–66 (2023)
23. Bruneau, M., et al.: A framework to quantitatively assess and enhance the seismic resilience of communities. Earthquake Spectra 19(4), 733–752 (2003)
24. Espinoza, S., Panteli, M., Mancarella, P., Rudnick, H.: Multi-phase assessment and adaptation of power systems resilience to natural hazards. Elect. Power Syst. Res. 136, 352–361 (2016)
25. Liu, X., Hou, K., Jia, H., et al.: A planning-oriented resilience assessment framework for transmission systems under typhoon disasters. IEEE Trans. Smart Grid 11(6), 5431–5441 (2020)
26. Liu, T., Zhang, Q., He, C.: Coordinated optimal operation of electricity and natural gas distribution system considering integrated electricity-gas demand response. Proc. CSEE 41(5), 1664–1676 (2021)
27. Zhang, T., Wang, J., Wang, H., Ruiyang, J., Li, G., Zhou, M.: On the coordination of transmission-distribution grids: a dynamic feasible region method. IEEE Trans. Power Syst. 38(2), 1857–1868 (2023)

28. Zhang, T., Wang, J., Li, G., et al.: Characterizing temporal-coupled feasible region of active distribution networks. In: 2021 IEEE Industry Applications Society Annual Meeting (IAS), pp. 1–7. IEEE, Piscataway, NJ (2021)
29. De Wolf, D., Smeers, Y.: The gas transmission problem solved by an extension of the simplex algorithm. Manage. Sci. 46. 1454–1465 (2000)
30. He, C., Dai, C., Wu, L., Liu, T.: Robust network hardening strategy for enhancing resilience of integrated electricity and natural gas distribution systems against natural disasters. IEEE Trans. Power Syst. 33(5), 5787–5798 (2018)
31. Chen, C., Wang, J., Qiu, F., et al.: Resilient distribution system by microgrids formation after natural disasters. IEEE Trans. Smart Grid 7(2), 958–966 (2016)
32. Chen, S., Liu, T., Dong, H., et al.: Generic layout optimization design methodology for China's loop-star natural gas field pipeline network, Nat. Gas Ind. B 11(5), 616–629 (2024)
33. Martínez Ceseña, E.A., Mancarella, P.: Energy systems integration in smart districts: robust optimization of multi-energy flows in integrated electricity, heat and gas networks. IEEE Trans. Smart Grid 10(1), 1122–1131 (2019)
34. He, C., Zhang, X., Liu, T., et al.: Distributionally robust scheduling of integrated gas-electricity systems with demand response. IEEE Trans. Power Syst. 34(5), 3791–3803 (2019)

How to cite this article: Chang, S., Li, G., Zhang, T., Zhou, M., Hong, Q., Wang, J.: Characterising the resilience of electro–hydrogen coupled system via convex hull estimation. Energy Convers. Econ. 1–13 (2025). https://doi.org/10.1049/enc2.70002

APPENDIX

A1 | Relaxation of the Weymouth equation

A method based on SOC relaxation and Taylor series was used for the Weymouth equation [32]. The coupled-system optimisation model is non-linear, non-convex, and difficult to solve using commercial solutions owing to the Weymouth equation. In this study, a simple mathematical transformation of the Weymouth equation was performed to transform it into an SOC equation, as shown in Equation (A1). The feasible region is on the surface of the SOC, which is still a non-convex problem. After relaxing Equation (A1), to obtain the SOC planning inequality constraint in Equation (A2), the feasible region becomes an SOC, which is transformed into a convex optimisation problem to be solved [33].

$$F_{mn,t}^2 + \left(K_{mn}\pi_{n,t}\right)^2 = \left(K_{mn}\pi_{m,t}\right)^2 \tag{A1}$$

$$F_{mn,t}^2 \le K_{mn}^2\left(\pi_{m,t}^2 - \pi_{n,t}^2\right) \tag{A2}$$

Equation (A2) is non-linear, which makes it difficult to solve and portray the EHCR. A Taylor series was used to transform the non-linear planning problem into a linear planning problem. Equation (A2) can be regarded as a function of the transmission pipeline flow with respect to the pressures at both ends of the node. Both sides of Equation (A2) are squared and a first-order Taylor series expansion is used to express Equation (A2) as the linearised function of any node pressure pair $(\pi_{m,t}^0, \pi_{n,t}^0)$ at both ends of the hydrogen pipelines, as Equation (A3) shows.

$$\begin{aligned} F_{mn,t} \le F_{mn,t}^0 + \frac{\partial F_{mn,t}}{\partial \pi_{m,t}}\left(\pi_{m,t} - \pi_{m,t}^0\right) + \\ \frac{\partial F_{mn,t}}{\partial \pi_{m,t}}\left(\pi_{n,t} - \pi_{n,t}^0\right) + \Delta F_{mn,t} \end{aligned} \tag{A3}$$

where $F_{mn,t}^0$ represents the hydrogen flow of the pipeline with pressure $\pi_{m,t}^0, \pi_{n,t}^0$ at both ends. $\Delta F_{mn,t}$ is the first-order residual term. Equation (A3) describes a cone in space after Taylor series expansion.

For any node pressure variation range $(\pi_m^{\min}, \pi_m^{\max})$, N expansion points are set to solve Equation (A3). As a hydrogen energy transmission network is typically radiant, the first pressure of the pressure pairs is higher than the end pressure. Equations (A4)–(A7) further describe the tangency of the linearised tangent plane to the taper. The contact point is on the line where the ratio between $\pi_{m,t}$ and $\pi_{n,t}$ is equal to the ratio between $\pi_{m,t}^i$ and $\pi_{n,t}^j$.

$$F_{mn,t} \le K_{mn}\left(\eta_{m,t}^i\pi_{m,t} - \eta_{n,t}^j\pi_{n,t}\right) \tag{A4}$$

$$\begin{cases} \pi_{m,t}^i \ge \pi_{n,t}^j \\ \pi_{m,t} \ge \pi_{n,t} \end{cases} \tag{A5}$$

$$\eta_{m,t}^i = \pi_{m,t}^i \Big/ \sqrt{\left(\pi_{m,t}^i\right)^2 - \left(\pi_{n,t}^j\right)^2} \tag{A6}$$

$$\eta_{n,t}^j = \pi_{n,t}^j \Big/ \sqrt{\left(\pi_{m,t}^i\right)^2 - \left(\pi_{n,t}^j\right)^2} \tag{A7}$$

where $\pi_{m,t}^i$ is the ith expansion point of the range $(\pi_m^{\min}, \pi_m^{\max})$, and $i = 1, 2, \ldots, N$. The accuracy of the proposed method was verified in reference [34], and when $N \ge 1000$, the computational error of the model is less than 0.001, which satisfies the network operation requirements. Therefore, N was set to 1000 in this study.

A2 | External cutting-plane solving algorithm

The objective in Equation (45) cannot be solved directly because it contains the origin problem variable x and dual variable z. However, if the constraints of x and z are decoupled, then Equation (45) can be expressed as Equation (A8).

$$\begin{aligned} f = \max_{z \in Z}\left[\boldsymbol{C}z + \max_{x}\left(-z^{\mathrm{T}}\boldsymbol{A}x\right)\right] \\ s.t.\ \boldsymbol{D}x \le d \ :\ v^{\mathrm{d}} \end{aligned} \tag{A8}$$

where v^{d} is a dual variable corresponding to the constraints of the resilient region. When the maximum problem $\max_x(-z^{\mathrm{T}}\boldsymbol{A}x)$ reaches optimal solutions, Equation (A8) can be deduced from the Karush–Kuhn–Tucker theorem (KKT).

$$\begin{cases} \boldsymbol{A}^{\mathrm{T}}z + \boldsymbol{D}^{\mathrm{T}}\,v^{\mathrm{d}} = 0 \\ v^{\mathrm{d}} \ge 0 \\ \boldsymbol{D}x \le d \\ v^{\mathrm{d}}\left(d - \boldsymbol{D}x\right) = 0 \end{cases} \tag{A9}$$

Based on the strong dual property, Equation (A9) can be rewritten as a dual problem to linearise the objective in Equation (A10). At this point, the original problem is transformed into a mixed-integer linear programming problem.

$$f = \max_{x,z,v^d} z^{\mathrm{T}}\boldsymbol{C} + \boldsymbol{D}^{\mathrm{T}}v^{\mathrm{d}}$$
$$s.t.\begin{cases} \boldsymbol{A}^{\mathrm{T}}z + \boldsymbol{D}^{\mathrm{T}}v^{\mathrm{d}} = 0 \\ \boldsymbol{B}^{\mathrm{T}}z = 0 \\ -1 \le z \le 0 \\ 0 \le v^{\mathrm{d}} \le M\partial \\ 0 \le d - \boldsymbol{D}x \le M(\partial - 1) \end{cases} \tag{A10}$$

where M denotes a sufficiently large constant. ∂ is a binary variable for decoupling x and z. Solving Equation (A10) implies that a vertex of the current resilience region can be obtained, which can determine a margin according to Equation (47).

It can be deduced from Equation (45) that if $\forall x \in \boldsymbol{\Omega}$, Equation (46) is valid. Otherwise, Equation (A11) is valid.

$$\exists z' \in \boldsymbol{Z}, z'^{\mathrm{T}}\boldsymbol{A}x < z'^{\mathrm{T}}\boldsymbol{C} \tag{A11}$$

As a result, when $\forall x \in \boldsymbol{\Omega}$, Equation (A12) is the boundary between the EHCR and non-EHCR, that is, the resilience margin.

$$z'^{\mathrm{T}}\boldsymbol{A}x = z'^{\mathrm{T}}\boldsymbol{C} \tag{A12}$$

Each vertex in the dual space corresponds to a resilience margin because the optimal solution z' reaches extreme values in dual space. Because of the excessive number of vertices in the dual space of the coupled system, an external cutting plane algorithm is proposed.

First, a sufficiently large space Ψ including the EHCR is set, and the solution of Equation (A10) must be $f(x^o) > 0$. x^o is the farthest vertex in space Ψ and is outside the EHCR. If any point x^i inside the EHCR makes $f(x^i) = 0$, the line x^{oi} connecting x^o and x^i must cross the resilience margin. The intersection x^b can be found on line x^{oi}, as shown in Equations (A13) and (A14).

$$x^b = \tau x^o + (1-\tau)x^i \tag{A13}$$

$$\tau = \frac{\rho\left(x^o, x^b\right)}{\rho\left(x^o, x^i\right)} \tag{A14}$$

where τ is the length parameter; $\rho(x^o, x^b)$ and $\rho(x^o, x^i)$ represent the distance between points.

Once the line x^{oi} is set, the intersection x^b of a length parameter τ can determine whether the x^b is on the resilience margin through solving Equation (A10). The external cutting-plane problem is transformed into a problem of searching for points on a settled line.